environmental microbiology

Environmental Microbiology (2013) **15**(3), 956–966 doi:10.1111/1462-2920.12039

Spatial mapping of extracellular oxidant production by a white rot basidiomycete on wood reveals details of ligninolytic mechanism

Christopher G. Hunt,[1]* Carl J. Houtman,[1] Don C. Jones,[1] Peter Kitin,[1,2] Premsagar Korripally[1,2] and Kenneth E. Hammel[1,2]

[1]*US Forest Products Laboratory, Madison, WI 53726, USA.*

[2]*Department of Bacteriology, University of Wisconsin, Madison, WI 53706, USA.*

Summary

Oxidative cleavage of the recalcitrant plant polymer lignin is a crucial step in global carbon cycling, and is accomplished most efficiently by fungi that cause white rot of wood. These basidiomycetes secrete many enzymes and metabolites with proposed ligninolytic roles, and it is not clear whether all of these agents are physiologically important during attack on natural lignocellulosic substrates. One new approach to this problem is to infer properties of ligninolytic oxidants from their spatial distribution relative to the fungus on the lignocellulose. We grew *Phanerochaete chrysosporium* on wood sections in the presence of oxidant-sensing beads based on the ratiometric fluorescent dye BODIPY 581/591. The beads, having fixed locations relative to the fungal hyphae, enabled spatial mapping of cumulative extracellular oxidant distributions by confocal fluorescence microscopy. The results showed that oxidation gradients occurred around the hyphae, and data analysis using a mathematical reaction–diffusion model indicated that the dominant oxidant during incipient white rot had a half-life under 0.1 s. The best available hypothesis is that this oxidant is the cation radical of the secreted *P. chrysosporium* metabolite veratryl alcohol.

Introduction

Microorganisms that use lignocellulose as a carbon source have an essential role in global carbon cycling, because most terrestrial carbon is fixed in this complex structural component of vascular plants or in humic substances derived from it. Lignocellulolytic organisms require oxidative mechanisms to disrupt lignin, the stereoirregular, non-hydrolysable, phenylpropanoid polymer that encases and protects the structural polysaccharides in lignocellulose (Kirk and Farrell, 1987; Boerjan *et al*., 2003). Basidiomycetes that cause white rot of wood are uniquely efficient at lignin degradation, and may employ a diverse array of ligninolytic oxidants (Kersten and Cullen, 2007; Hatakka and Hammel, 2010). For example, four mechanisms have been proposed for the most intensively studied white rot fungus, *Phanerochaete chrysosporium*:

Hypothesis I: Fe(III) oxalate chelates in lignocellulose may be reduced to Fe(II) oxalate chelates by secreted cellobiose dehydrogenase (CDH) (Kremer and Wood, 1992; Henriksson *et al*., 2000) or by various glycopeptides (Tanaka *et al*., 1999). This Fe(II) may then undergo the Fenton reaction with hydrogen peroxide, which is produced either by secreted fungal oxidases or by Fe(II) auto-oxidation (Park *et al*., 1997; Kersten and Cullen, 2007), to generate ligninolytic hydroxyl radicals ($H_2O_2 + Fe^{2+} + H^+ \rightarrow H_2O + Fe^{3+} + \bullet OH$).

Hypothesis II: Secreted manganese-dependent peroxidases (MnPs) may react with H_2O_2 and Mn(II) organic acid chelates in lignocellulose to produce Mn(III) organic acid chelates, mild oxidants that can cleave the minor phenolic structures in lignin (Wariishi *et al*., 1989). Additionally, MnPs and the Mn(III) they produce oxidize a variety of surrounding molecules such as organic acid chelators of Mn(III) and unsaturated lipids to generate potentially ligninolytic reactive oxygen species that include certain peroxyl radicals (•OOR) (Popp *et al*., 1990; Kapich *et al*., 1999).

Hypothesis III: Lignin peroxidases (LiPs) in the presence of H_2O_2 may abstract electrons from aromatic rings of the predominant non-phenolic structures in lignin, thus catalysing ligninolysis directly by generating scissile cation radical intermediates in the polymer (Tien and Kirk, 1984; Harvey *et al*., 1985; Kersten *et al*., 1985; Hammel *et al*., 1986).

Hypothesis IV: LiPs may oxidize veratryl alcohol (3,4-dimethoxybenzyl alcohol), a secreted *P. chrysosporium* metabolite, to produce the veratryl alcohol cation radical,

Received 26 October, 2012; accepted 1 November, 2012. *For correspondence. E-mail cghunt@fs.fed.us; Tel. (+1) 608 2319521; Fax (+1) 608 2319262.

which could then diffuse into the lignin and cleave it oxidatively by the same electron transfer mechanism that LiPs employ when they act directly (Harvey *et al*., 1986; Candeias and Harvey, 1995; Bietti *et al*., 1998).

Many studies have provided evidence that white rot fungi express components of the above systems in biodegrading lignocellulose. For example, mRNAs encoding CDH, MnPs, and LiPs have been detected in wood undergoing decay by *P. chrysosporium* and related fungi (Janse *et al*., 1998; Vallim *et al*., 1998; Martinez *et al*., 2004; Sato *et al*., 2009; MacDonald *et al*., 2011; Fernandez-Fueyo *et al*., 2012; MacDonald and Master, 2012). Some of the corresponding proteins have also been observed in wood cultures using proteomic methods (Sato *et al*., 2007; Ravalason *et al*., 2008; Mahajan and Master, 2010; Vanden Wymelenberg *et al*., 2010; Manavalan *et al*., 2011; Adav *et al*., 2012; Fernandez-Fueyo *et al*., 2012) and by electron microscopy with immunolabelling (Daniel *et al*., 1989; 1991). However, little is known about the extent to which these oxidative systems actually function in biodegrading wood, and it remains difficult to determine which are quantitatively most important.

To address these questions, it would be useful if oxidative activity could be imaged on lignocellulosic specimens undergoing incipient decay. In this way, data on the extent and spatial distribution of oxidation around individual fungal hyphae could be obtained. The resulting activity maps might then point to a specific mechanism, because the agents proposed in hypotheses I–IV are expected to vary with respect to their rates of diffusion from the hyphae and rates of reaction with their surroundings.

We have attached an oxidant-sensing fluorescent dye to micrometre-scale silica beads, added these probes to wood specimens, and inoculated the wood with *P. chrysosporium*. Since the beads remain stationary on the wood, the immobilized dye molecules have fixed locations relative to the fungal hyphae. This approach allows spatial mapping of cumulative oxidative activity in the specimens by confocal fluorescence microscopy. Our analyses of the resulting data show that hypothesis IV best explains the oxidative system that operates during the earliest stage of biodegradation.

Results

Fluorescent bead preparation

To enable detection of as many different fungal oxidants as possible, we chose a relatively non-selective, easily oxidizable dye, BODIPY 581/591 (Drummen *et al*., 2004), for immobilization. This dye excites maximally at 581 nm and fluoresces at 591 nm (red) in its native reduced form. It excites maximally at 488 nm and fluoresces at 523 nm (green) when oxidized (Fig. 1). The fact that its reduced and oxidized forms both exhibit visible fluorescence makes BODIPY 581/591 a ratiometric detector, i.e. the extent of bead oxidation can be estimated from the red/green (RG) ratio.

We tethered the BODIPY to amino-terminated 3 μm-diameter silica beads via amide linkages (Fig. 1). The beads carried dye molecules both on their periphery and in their pores (Fig. S1a), and the pore size (100 Å) was large enough to admit all agents under consideration, including enzymes. For additional details on the beads' physical properties, see the *Supplementary notes*. To calibrate the beads' response to oxidative events, we oxidized them *in vitro* with various amounts of peroxyl radicals generated from 2,2′-azobis(2-methylpropionamidine) dihydrochloride (AAPH) (Krainev and Bigelow, 1996), and then determined the resulting RG ratios by fluorescence microscopy (Fig. S1b).

Reactivity of beads with proposed oxidants

BODIPY 581/591 has already been used as a general detector of reactive oxygen species, and both hydroxyl and peroxyl radicals are known to oxidize it (see hypotheses I and II) (Drummen *et al*., 2004). To check whether the dye can also detect other oxidants with a proposed role in white rot, we treated our BODIPY beads with H_2O_2 and purified *P. chrysosporium* ligninolytic peroxidases.

As shown in Fig. 2, the beads were not oxidized by H_2O_2 alone, but were oxidized by the combination of H_2O_2 and LiP (see hypothesis III). The ability of LiP to oxidize this very hindered substrate without involvement of a diffusible redox mediator presumably reflects the fact that electron abstraction from donor substrates occurs not in the LiP haem cleft, but rather at an exposed tryptophan

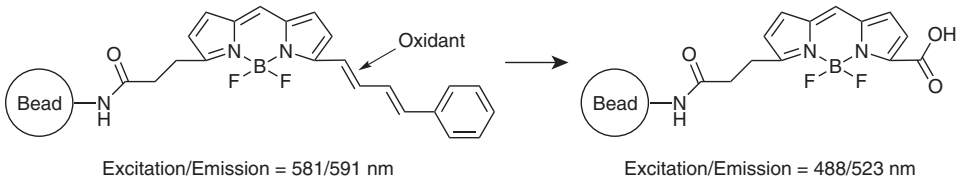

Fig. 1. Schematic of bead-linked BODIPY 581/591, showing site of oxidative cleavage.

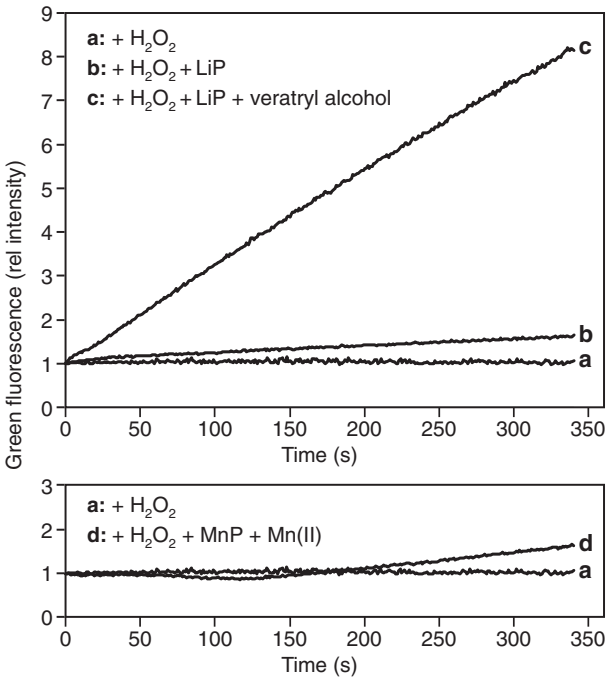

Fig. 2. Increases in green fluorescence of BODIPY beads due to oxidation by purified *P. chrysosporium* peroxidases. The upper panel shows results obtained with LiP, and the lower panel shows results obtained with MnP. The control reaction without enzyme is the same in both panels. Reaction ingredients were as noted on the graph.

residue located on the enzyme surface (Blodig *et al.*, 1998). Also shown in Fig. 2 is the effect of adding 3 mM veratryl alcohol to the assay with LiP. The resulting faster rate of bead oxidation likely indicates that the cation radical produced when LiP oxidizes veratryl alcohol is able to serve as a redox mediator between the enzyme and the sterically hindered bead-linked BODIPY molecule (see hypothesis IV) (Harvey *et al.*, 1985; Candeias and Harvey, 1995; Bietti *et al.*, 1998). However, the data do not exclude the possibility that stimulation by veratryl alcohol instead reflects its ability to serve as an alternate electron donor that allows LiP to turn over faster, thus facilitating its ability to oxidize recalcitrant substrates (Koduri and Tien, 1994).

We also observed that the BODIPY beads were oxidized by MnP in the presence of H_2O_2, provided the reaction also contained Mn(II) and an organic acid chelator of Mn(III), both of which are required for MnP turnover (Wariishi *et al.*, 1992). Figure 2 shows that bead oxidation occurred but was preceded by a lag when we used tartrate as the Mn(III) chelator. Notably, the formation of Mn(III) tartrate, which gives a diagnostic visible absorption spectrum (Wariishi *et al.*, 1992), occurred without any lag in these reactions (data not shown). We obtained similar results using oxalate (data not shown), which may be the physiological Mn(III) chelator (Kuan and Tien, 1993). These results suggest that diffusible Mn(III) chelates, which are the initial products of MnP catalysis, do not oxidize BODIPY directly. Instead, the proximal oxidants of BODIPY in MnP-catalysed reactions are likely peroxyl and perhydroxyl radicals, which are produced when Mn(III) oxidizes the organic acid that chelates it (Taube, 1948; Levesley and Waters, 1955; Popp *et al.*, 1990) (see hypothesis II).

In summary, although it is not always possible to identify the proximal oxidant of a LiP or MnP substrate unambiguously in enzymatic assays, our results and prior work (Drummen *et al.*, 2004) indicate that all the ligninolytic agents proposed for *P. chrysosporium* can oxidize BODIPY 581/591 by some route. Therefore, we proceeded with physiological experiments using *P. chrysosporium* and BODIPY beads on biodegrading wood.

Summary of culture system

We used 40 μm-thick tangential sections of spruce sapwood, each weighing approximately 7 mg (dry wt), as the substrate for fungal growth. The sections were embedded in a small volume of agar containing a dispersion of BODIPY beads (Fig. 3a), such that all wood cell lumens were filled. The primary purpose of the agar, a poor carbon source for *P. chrysosporium* and most other fungi, was to fix the beads in position relative to the growing fungus and the wood. The cultures were inoculated at one edge of the wood section and incubated for 3–4 days until hyphae had grown across the specimens,

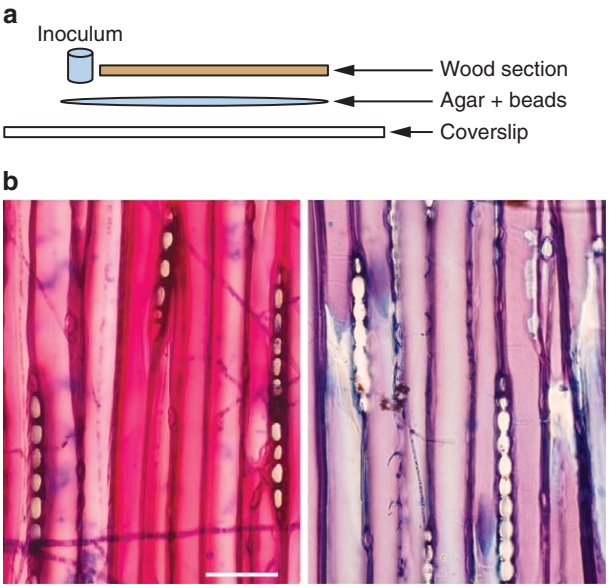

Fig. 3. a. Exploded schematic of fungal culture system.
b. Wood sections recovered and stained with safranin plus astra-blue after colonization with *P. chrysosporium*. Left: 2 day culture. Right: 4 week culture. The scale bar indicates 50 μm.

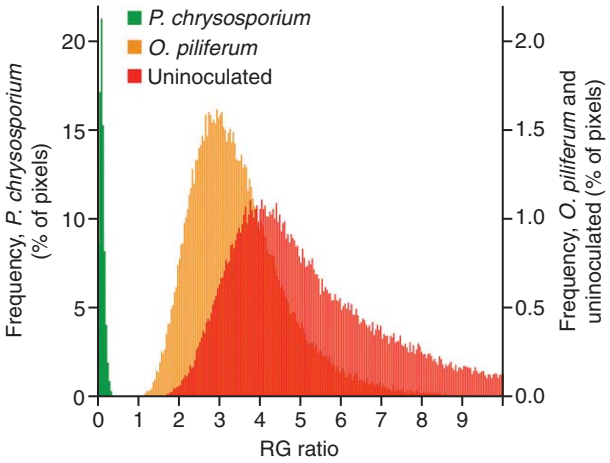

Fig. 4. Histograms showing RG ratio distributions for beads in uninoculated cultures, *O. piliferum* cultures, and *P. chrysosporium* cultures after 4 days at 28°C. For each treatment, three cultures were examined to obtain eight images, which together provided a total of at least 3.4×10^4 pixels.

at which point most were harvested for imaging of BODIPY beads and hyphae between the wood and coverslip by confocal microscopy.

Biodegradative competence

In addition, some specimens were incubated for 4 weeks to determine whether the culture system would elicit expression of the ligninolytic system in *P. chrysosporium*. Figure 3b shows light microscopy results for recovered wood sections that had been stained with both safranin, which stains lignin red, and astra-blue, which stains cellulose blue (Srebotnik and Messner, 1994). In recently inoculated specimens, only red staining was apparent because the lignin in sound wood shields the cellulose, preventing penetration by astra-blue. By contrast, purple staining indicative of partial delignification was evident in specimens colonized by *P. chrysosporium* for 4 weeks. In addition, structural damage to ray cell walls, tracheid walls, pit chambers and pit membranes was apparent in the inoculated wood after 4 weeks.

Reactivity of beads in cultures

As BODIPY is easily oxidized, and all living cells produce some extracellular reactive oxygen species via peroxidation of their outer membrane lipids (Halliwell and Gutteridge, 1999), it was also necessary to determine whether the bead-linked BODIPY dye was sufficiently robust to resist oxidation in a non-ligninolytic fungal culture. We compared bead oxidation on wood specimens colonized by *P. chrysosporium* with oxidation on specimens colonized by the lignicolous ascomycete *Ophiostoma piliferum*. The latter fungus is non-ligninolytic, but grows to some extent on wood by consuming its lipids and other extractives (Farrell *et al.*, 1993). Examining areas of the colonized wood that contained similar hyphal densities, we observed that after 4 days almost all the beads in the *P. chrysosporium* cultures had been oxidized. By contrast, *O. piliferum* caused only a small shift in the beads' RG ratio distribution relative to the distribution exhibited by uninoculated cultures (Fig. 4).

Development of mathematical model

The question we aimed to address is whether information about the *P. chrysosporium* oxidant that predominates during incipient wood decay can be inferred from the distribution of oxidation around hyphae on a colonized wood specimen. One possibility was that the beads we employed as sensors might be more oxidized when near the fungus, thus leading to gradients of RG ratios around the hyphae. Alternatively, the extents of sensor oxidation might exhibit no spatial relationship with the hyphae.

The extents of oxidation registered by the beads are cumulative, i.e. their RG ratios are related to integrals of oxidative events over time. Three variables influence how these integrals vary with time and distance from a source of oxidant production: (i) the rate D at which the oxidants diffuse, (ii) the rate K at which the oxidants decay, and (iii) the amount of time t that the system has been producing oxidants. Gradients are steeper if the oxidant diffuses slowly or decays quickly, and are conversely flatter if the oxidant diffuses quickly or decays slowly. Observed gradients also become flatter with longer time as the sensors approach a completely oxidized state, because at that point their fluorescence stops changing colour.

Although the extent of oxidation around a hypha is a complex function of all the above factors, insight can be obtained from a mathematical reaction–diffusion model (Cussler, 1984). Given particular reaction and diffusion rate constants for a proposed oxidant, such a model predicts gradients in oxidation at various times. The resulting predictions can then be compared with experimental observations on extents of sensor oxidation around hyphae collected from a statistically valid sample of bead images. The comparison reveals whether the data can be fit to the model for any time that falls within the length of the experiment.

To predict the reaction–diffusion properties of the principal oxidants involved in hypotheses I–IV, we needed estimates of their values for D and K. These we obtained using a combination of literature values, correlations, and extrapolations (see *Experimental procedures* and *Supplementary notes*). Small molecules such as chelated metal ions or the veratryl alcohol cation radical are expected to have values of D near 10^{-5} cm^2 s^{-1} in water, whereas

large globular molecules such as enzymes have D near 10^{-7} cm^2 s^{-1} (Cussler, 1984). Diffusion coefficients in agarose gels are between 30% and 90% of the values in water and can be estimated from literature values (Olsson *et al*., 1992; Fatin-Rouge *et al*., 2003). Values of K for the oxidants under consideration reflect their disproportionation or reaction with the surroundings and range from roughly 10^{-4} per second to 10 per second (Taube, 1948; Candeias and Harvey, 1995; Park *et al*., 1997; Bietti *et al*., 1998). Table 1 summarizes our estimates.

Development of equations for the reaction–diffusion model requires some assumptions about the physical system. We have assumed that (i) oxidants are produced at the surface of cylindrical hyphae that have a 2 μm diameter and are much longer than they are wide, (ii) the surrounding medium is axially symmetric around the hyphae and uniform in diffusion properties, (iii) other hyphae surround a given hypha at a uniform distance 2R of 80 μm and produce similar levels of oxidant over the life of the experiment, and (iv) a single type of oxidant dominates the reactions with sensor beads. The purpose of the last assumption is not to presuppose that the fungus actually employs only one ligninolytic mechanism at a time, but rather to consider each proposed mechanism by itself mathematically so its individual contribution to the distribution of oxidants around the fungus can be assessed. The translation of the assumptions into mathematical form is discussed in the complete derivation (see *Supplementary notes*).

Our analysis shows that two dimensionless terms are important in the model. One of these can be defined as dimensionless time τ, and indicates how well-developed the concentration profiles are.

$$\tau = \frac{tD}{R^2}$$

A small value for τ corresponds to the time when the hypha has just begun to secrete oxidants. At this point, the concentration profile is still developing, which is expected to cause a transient oxidation gradient. However, as τ becomes larger, the spatial distribution of oxidant concentration around the hypha approaches a dynamic steady state, after which any observed gradient is non-transient. The initial stages of the concentration profile are governed by a mathematical term of the form $e^{-\tau}$, so for $\tau = 5$ the system is already within 1% of its steady-state profile. Given $R = 40$ μm, one can calculate the time required to arrive within 1% of steady-state for the various oxidants as shown in Table 1. The results show that even for the slowest moving oxidant, LiP, the required time is less than 2 min. A steady state assumption is accordingly reasonable for our model because, even if the oxidant concentration at the hyphal surface changes markedly during an

Table 1. Diffusion and decay properties for proposed ligninolytic agents.

Hypothesis	Agent[a]	Mol wt (Da)	10^{-6} D_w[b] (cm^2 s^{-1})	D_g/D_w	10^{-6} D_g[b] (cm^2 s^{-1})	Time to steady state profile (s)	Major fate	K (s^{-1})	$t_{1/2}$ (s)	θ[c]
I	[Fe(II) oxalate]^0	144	22.90	0.27	6.17	13	Fenton reaction with H_2O_2 (Park *et al*., 1997)	0.0232	29.8	0.25 ± 0.07
II	[Mn(III) oxalate]$^+$	143	26.00	0.27	7.00	11	Disproportionation to $CO_2^{\bullet-}$, CO_2, and Mn(II) (Popp *et al*., 1990)	0.00178	389	0.06 ± 0.01
III	LiP	4×10^4	1.09	0.68	0.74	108	Denaturation (Koduri and Tien, 1994)	0.00019	3600	0.06 ± 0.03
IV	[Veratryl alcohol]$^{+\bullet}$	168	10.53	0.90	9.48	8	Reaction with H_2O to produce benzylic radical (Bietti *et al*., 1998)	39.5	0.018	8.2 ± 1.2

a. Although the agents proposed for hypothesis II–IV are oxidants, Fe(II) acts as a reductant in hypothesis I. However, subsequent reactions of the hypothesis I Fenton oxidant are extremely rapid (Halliwell and Gutteridge, 1999), so for brevity we refer in the text to all proposed ligninolytic agents as oxidants.
b. D_w, diffusion coefficient in water; D_g, diffusion coefficient in agarose gel.
c. Values of θ are given ± 95% confidence intervals, which were obtained using estimates of uncertainty in D_g and K as described in the *Supplementary notes*.

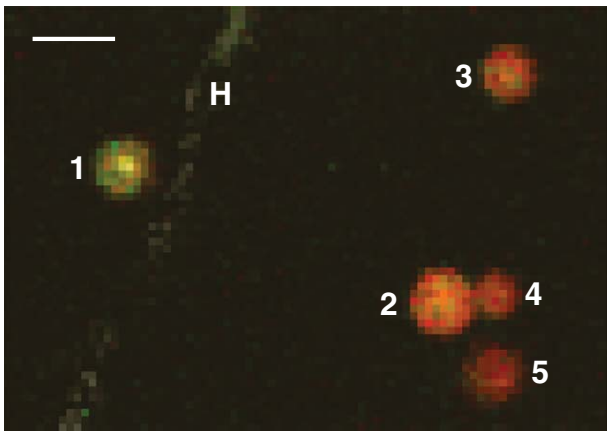

Fig. 5. Image of a *P. chrysosporium* hypha (H) growing on a wood section, showing a nearby oxidized green bead (1), two more distant partially oxidized orange beads (2, 3), and two yet more distant, slightly oxidized red beads (4, 5). The scale bar indicates 5 μm.

experiment, the concentration profile in the surrounding medium follows these changes very quickly.

The other term central to the mathematical model is the reaction–diffusion ratio θ, which indicates whether reaction or diffusion dominates the oxidant concentration profile relative to the position of the hypha.

$$\theta = \sqrt{\frac{KR^2}{D}}$$

Given a steady state assumption, the parameter θ completely determines the analytical solution for the profiles of oxidant concentration as a function of distance from the hypha, as shown by the three examples plotted in Fig. S2. For values of θ greater than 1, the reaction rate dominates and the concentration gradient is relatively steep. For values of θ less than 1, diffusion dominates and the gradient is relatively flat. Table 1 shows our calculated values of θ for hypotheses I–IV. It is clear that the system based on the veratryl alcohol cation radical is the only one expected to exhibit gradients in sensor oxidation. The other three systems generate oxidants so long-lived that they become uniformly distributed before they decay.

Distribution of bead fluorescence in biodegrading wood specimens

With the fluorescence colour channels turned off to prevent selection bias, we examined 3 day *P. chrysosporium* cultures on spruce wood sections for hyphae and nearby beads that met our imaging criteria (see *Experimental procedures*). An extensive search identified 13 such hyphae associated with a total of 56 beads. The low number discovered chiefly reflects our requirement that no other hypha be detectable within 80 μm of the hypha selected, either in the plane imaged or in the planes above and below.

When fluorescence images of the selected regions were subsequently analysed, it appeared that beads closer to the hyphae were more oxidized than those more distant (Fig. 5). To test this hypothesis, the 56 beads around the 13 hyphae were subjected to statistical analysis. We divided the beads near each hypha into two balanced groups, one closer to the hypha and one farther away, and determined the average RG ratio for each group. By comparing these averages we observed that in all 13 cases the group nearer the hypha had a lower RG ratio. Since the probability of this result occurring at random is 0.012%, we concluded that oxidation gradients occurred around the hyphae.

Fit of oxidation data to the model

Using our reaction–diffusion model and the calibration curve that relates RG ratios to the number of oxidative events in the medium surrounding the beads (Fig. S1b), we predicted RG ratios as a function of distance from the hypha for various values of θ. We then fit the imaging data to the value of θ that minimized the square of the difference between the model and the data. In addition, since we do not know how long each hypha had been producing oxidant when it was imaged, we allowed t to take on values, one corresponding to each hypha, that minimize this square difference. The result of the minimization gave a value for θ of 3.6 with a 95% confidence interval of 1.0–10.1. As shown in Table 1, only hypothesis IV, in which the veratryl alcohol cation radical acts as the proximal oxidant, gives a θ-value (8.2 ± 1.2) within this confidence interval.

Although all data from the 13 hyphae were put into our model to obtain the above value for θ, it is easiest to visualize the results graphically by looking at subgroups of the data. Figure 6a shows plots of the RG ratios against distance from the hypha for beads associated with two groups: the four hyphae whose beads exhibited the highest average RG ratio, and the four hyphae whose beads exhibited the lowest average RG ratio. Our calculated value of 3.6 for θ, which agrees with hypothesis IV, gives curves that fit the two plots well. It also gives reasonable average values of t: 0.36 h for the high RG ratio group (95% confidence interval 0.26–0.50 h), and 15.5 h for the low RG ratio group (95% confidence interval 12.0–21.3 h).

By contrast, it is impossible to fit curves well to all the selected data using values of θ that correspond to hypotheses I–III. For example, $\theta = 0.06$, which corresponds to LiP acting without a radical mediator or to oxidation by the Mn(III) monooxalate complex, yields the predictions shown in Fig. 6b. The low RG ratio data are adequately fit by the model in this case, since all hypotheses yield flat gradients once the beads have become heavily oxidized,

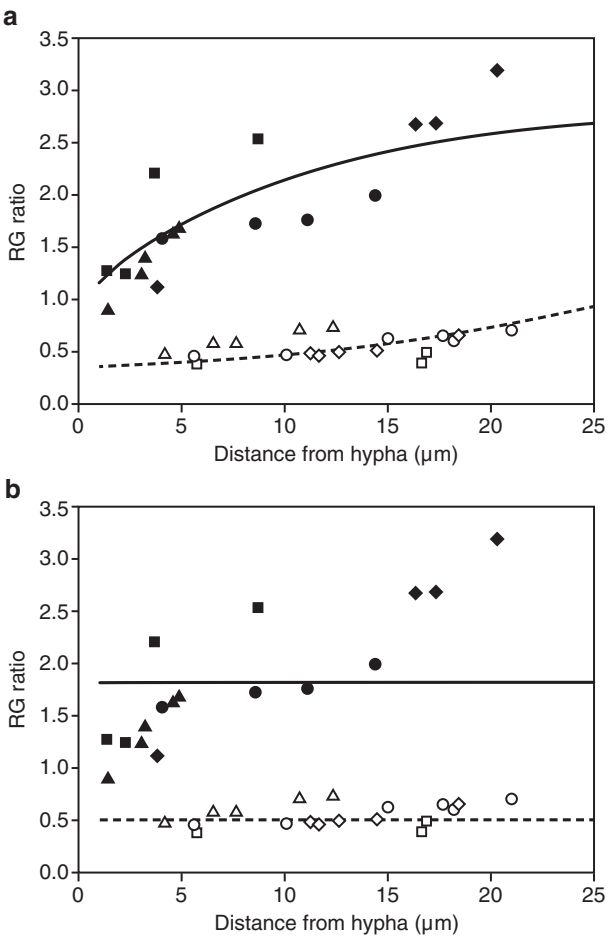

Fig. 6. Fits of selected RG ratio data from colonized wood sections to the reaction–diffusion model. Each different plot symbol specifies values for beads around a particular hypha.
a. Freely diffusing veratryl alcohol cation radical as the oxidant with $\theta = 3.6$. The upper solid curve is for $t = 0.36$ h and the lower dashed curve is for $t = 15.5$ h.
b. Freely diffusing LiP or Mn(III) oxalate as the oxidant with $\theta = 0.06$. The upper solid curve is for $t = 0.36$ h and the lower dashed curve is for $t = 7$ h.

but the pronounced gradient evident in the high RG ratio data cannot be well fit using any value of *t*.

Discussion

In our experiments, the white rot fungus *P. chrysosporium* oxidized bead-linked BODIPY on wood to a much greater extent than did the non-ligninolytic wood-inhabiting fungus *O. piliferum*. This finding, in combination with our observation that *P. chrysosporium* subsequently delignified the wood, suggests that our sensor beads detected the production of ligninolytic oxidants by the white rot fungus. Specifically, our imaging data and modelling show that the predominant oxidant produced by *P. chrysosporium* on wood during the earliest stage of biodegradation was a species that diffused from the hyphae and had a half-life under 0.1 s (Table 1). This oxidant could be an agent that remains to be discovered, but our analysis fits an existing hypothesis well: veratryl alcohol cation radicals may be produced by LiPs on wood, where they subsequently act as diffusible ligninolytic oxidants (Harvey *et al.*, 1985; Candeias and Harvey, 1995; Bietti *et al.*, 1998).

An important caveat is that the LiPs must remain associated with the fungal hyphae for this hypothesis to apply, because no gradients can occur if the enzymes diffuse freely within the sample. However, this requirement appears reasonable because electron microscopic studies have shown that LiPs are predominantly present on the hyphal surface rather than throughout the wood cell lumen during early decay (Daniel *et al.*, 1989). An additional qualification is that our results do not rule out the simultaneous presence of diffusible, long-lived oxidants that exhibited no gradients. Rather, they show that these oxidants, if present, oxidized the BODIPY beads to such a small extent during incipient decay that their contribution did not obscure the gradients displayed by the dominant species our experiments detected. Finally, it is important to note that a different mixture of oxidants, including freely diffusible LiPs, MnPs, and less-studied enzymes, likely have a role under other environmental conditions or at later stages of oxidative attack on wood by *P. chrysosporium*.

A key question is whether the quantities of oxidant we observed in our cultures were significant relative to the quantity required to initiate biodegradation of the wood. Our results showed that in 4 days *P. chrysosporium* produced enough oxidant that the RG ratios of almost all beads on a specimen exceeded the range of our standard curve, which extended to 61 mM AAPH-derived radicals (Fig. S1b). Thus, a typical culture containing 80 μl of water produced at least 5 μmol of nominal peroxyl radical equivalents in 4 days. This value can be compared with the total number of *c.* 200 Da lignin, cellulose, and hemicellulose subunits in a 7 mg spruce wood specimen, which is about 35 μmol. Although this comparison is highly approximate, it is clear that the amount of oxidant produced by the fungus was stoichiometrically significant.

Experimental procedures

Organisms and reagents

Phanerochaete chrysosporium monokaryotic strain RP-78 (ATCC MYA-4764) (Martinez *et al.*, 2004) was obtained from the Center for Forest Mycology, US Forest Products Laboratory. The Cartapip strain of *O. piliferum* (Farrell *et al.*, 1993) was a generous contribution from B. W. Held at the University of Minnesota. Both fungi were maintained on potato dextrose agar. Reagent grade chemicals were obtained from Sigma/Aldrich (St Louis, MO, USA) unless otherwise stated.

Production of fluorescent beads

We coupled the fluorescent ratiometric dye BODIPY 581/591 via amide linkages to highly porous amino-terminated silica beads that are ordinarily used for high-performance liquid chromatography (Luna NH_2, 3 μm particle size, 100 Å pore diameter, 400 $m^2\ g^{-1}$ surface area, Phenomenex, Torrance, CA, USA). We then acetylated the remaining amino groups so the beads would not carry a net positive charge under the acidic conditions (pH ≈ 4) produced during white rot. A 50 mg quantity of the beads was combined with 1.4 ml of dry isopropanol and the resulting suspension was added to 312 nmol of BODIPY 581/591 succinimidyl ester (BODIPY 581/591 SE, Invitrogen, Carlsbad, CA, USA) that had been dissolved beforehand in 0.9 mol of dry *N,N*-dimethylformamide. The suspension was shaken for 1 h in the dark at room temperature, after which 5 ml of acetic anhydride was added and the suspension was shaken for 5 min. The beads were then rinsed several times with isopropanol and stored in the dark as an isopropanol suspension at –80°C to prevent auto-oxidation.

Fluorescence spectroscopy

Fluorescence from beads was monitored with a SPEX Fluorolog Tau-2 fluorescence spectrometer (Jobin Yvon, Edison, NJ), using a 5 nm bandpass for both excitation and emission. Green fluorescence was measured at 515 nm with 488 nm excitation, and red fluorescence at 600 nm with 575 nm excitation. Fluorescence resonance energy transfer (FRET) was monitored by comparing the 600 nm emission intensities obtained by excitation at 488 nm vs 575 nm. Dye concentration on BODIPY beads was estimated by comparing the red fluorescence intensity of stirred beads in methanol with the red fluorescence intensity of free BODIPY 581/591 succinimidyl ester that had been dissolved in methanol.

Enzymatic assays

LiP isozyme H2 was produced in nitrogen-limited *P. chrysosporium* cultures and chromatographically purified to apparent homogeneity as described (Tien and Kirk, 1988). It contained no detectable MnP activity. MnP isozyme H4 was produced by heterologous expression in *Aspergillus oryzae* and chromatographically purified to apparent homogeneity as described (Stewart *et al*., 1996). It contained no detectable LiP activity. LiP activity using veratryl alcohol as the substrate (Tien and Kirk, 1988) and MnP activity using 2,6-dimethoxyphenol as the substrate (Wariishi *et al*., 1992) were measured as described, where one unit of activity converts 1 μmol of substrate per min.

Activities against BODIPY beads were assayed as follows. (i) Activity due to LiP: 180 μg of beads and 0.1 unit of LiP isozyme H2 in a final volume of 1.80 ml of sodium tartrate buffer (20 mM, pH 4.5) were stirred at ambient temperature in a quartz fluorescence cuvette. H_2O_2 (0.4 mM) was added to start the reaction and the increase in fluorescence at 515 nm was monitored over time as described above. (ii) Activity due to LiP assisted by veratryl alcohol: The assay was conducted as for LiP alone, but with the addition of 3 mM veratryl alcohol. (iii) Activity due to MnP: The assay was conducted in the same way, except that 0.2 unit of MnP isozyme H4 was used as the enzyme, 2 mM $MnSO_4$ was included, and veratryl alcohol was omitted.

Culture conditions

Cultures were grown on microtomed tangential sections of spruce sapwood (*Picea glauca*, 40 mm long, 10 mm wide, 40 μm thick; dry wt approximately 7 mg) that were embedded in agar containing a nitrogen/mineral salts medium and BODIPY beads. The purpose of the agar was to immobilize the beads next to the wood specimen and also to prevent desiccation of the specimen during fungal growth. The medium consisted of 0.8% agar in modified low nitrogen BIII medium containing the standard level of trace elements (Tien and Kirk, 1988). The modifications were that glucose was omitted, ammonium nitrate replaced ammonium tartrate as the nitrogen source, and sodium polyacrylate (0.36 g l^{-1}, 250 kDa molecular mass, pH 4.5) replaced sodium 2,2-dimethylsuccinate as the buffer.

To set up cultures, a suspension of BODIPY beads was separated from its isopropanol by decantation and resuspended in water. A 5 μl portion of the water suspension containing 0.017 mg of beads was then placed on a glass coverslip (22 by 60 mm) that was kept on a 45°C table throughout the procedure. Without delay, 75 μl of warm liquid agar medium was added with mixing, followed by an autoclaved wood section. A Teflon sheet followed by a 100 g weight were then placed atop the assembly, which was then removed from the heated table.

After solidification of the agar, the weight and Teflon sheet were removed, and a 5 mm diameter potato dextrose agar plug containing mycelium of *P. chrysosporium* or *O. piliferum* was placed next to the wood at one of its 10 mm wide edges. The inoculum agar plugs were cut from the advancing hyphal fronts of recently inoculated culture plates. For experiments to search for gradients in bead oxidation, *P. chrysosporium* was grown on the wood sections for 72 h at 38°C and 100% relative humidity. Under these conditions, uninoculated control specimens auto-oxidized to about the same extent as that produced by treatment with 17 mM of AAPH-derived radicals, and therefore data obtained from inoculated cultures were corrected for this contribution. For experiments to compare extents of bead oxidation by *P. chrysosporium* and *O. piliferum*, both fungi were grown on the wood sections for 96 h at 28°C and 100% relative humidity. Under these conditions, bead auto-oxidation was negligible.

To measure hyphal density after growth of *P. chrysosporium* and *O. piliferum*, colonized wood sections were imaged in the confocal microscope from the coverslip to 56 μm deep at 4 μm intervals. Using the Image J program, a computer mouse was used to trace the length of all hyphae visible in reflectance mode, and the total hyphal length in each $325 \times 325 \times 56$ μm region was summed. A minimum of nine areas comprising three areas of three wood sections was imaged for each fungus and culture condition.

Light microscopy

The progress of lignocellulose decay in specimens was followed by light microscopy after staining with safranin and

astra-blue. We used the staining protocol of Srebotnik and Messner (1994) with some modifications (see *Supplementary notes*) because our wood sections were relatively thick at 40 μm.

Fluorescence microscopy

Confocal imaging was used to observe beads and fungal hyphae on the wood sections. Imaging was done on a Zeiss 510 Meta confocal laser scanning microscope, using a 1.2 numerical aperture (NA) 40× water objective. Images were acquired in 2 μm thick optical sections with 12 bit resolution and a pixel width of 0.45 μm. Green (oxidized dye) emission was recorded at 500–550 nm with 488 nm excitation and red (reduced dye) emission was recorded at ≥ 560 nm with 543 nm excitation. The intensities of the two excitation wavelengths were varied independently and were increased to observe more highly oxidized samples. For additional explanation, see the *Supplementary notes*.

Fluorescence image analysis

Image manipulation was performed with the ImageJ program (available at http://rsb.info.nih.gov/ij). Pixels were selected that had sufficient green intensity to exclude fluorescence background and that were not saturated in the green or red channels. The black background count was then subtracted from both channels, and the red channel intensity was divided by the green channel intensity to get an initial RG ratio. The final RG ratio was obtained by adjusting the initial ratio for relative laser intensity.

Criteria for gradient analysis

For each analysis, an isolated hypha in good focus was chosen from an area of the wood having at least 18 mm of hyphal length per square millimetre. The hypha was accepted for further analysis only if the following additional criteria were met: (i) No other hypha was detectable within 80 μm in any dimension. (ii) Beads around the hypha were in the same image plane and provided at least 14 pixels of non-overlapping data. (iii) Every bead was located in the same wood cell lumen as the hypha. To prevent selection bias, areas for gradient analysis were selected with the fluorescence colour channels off.

Calibration of beads

Wood specimens were embedded in agar-containing medium on coverslips by the standard procedure except that the fungal inoculum was omitted and the free radical initiator AAPH was added to the agar at concentrations of 0, 6.5, 17, 35, and 64 mM. After incubation at 38°C for 3 days, the specimens were imaged and their average RG ratios determined. The quantity per volume of AAPH-derived peroxyl radicals expected at each AAPH concentration was determined spectrophotometrically at 368 nm by monitoring the AAPH decay rate in solution at 29°C and pH 4.5 as described by Krainev and Bigelow (Krainev and Bigelow, 1996). The half-life of AAPH under these conditions was 437 h (95% confidence interval, 412–445 h). The rate constant for AAPH thermolysis at 38°C was estimated by extrapolating the value measured at 29°C using an activation energy of 114.6 kJ mol^{-1} (Henriquez *et al*., 2002). The standard curve for beads calibration (Fig. S1b) was then prepared by plotting the expected quantity per volume of peroxyl radicals against the observed RG ratios for the specimens. See the *Supplementary notes* for additional explanation.

Acknowledgements

We thank Vitaliy Timokhin for syntheses of BODIPY beads. This work was supported by grants DE-AI02-07ER64491 (C. G. H. and K. E. H.) and DE-SC0006929 (K. E. H., C. G. H., and C. J. H.) from the U.S. Department of Energy, Office of Biological and Environmental Research. Confocal imaging was performed at the Plant Imaging Center, Department of Botany, University of Wisconsin-Madison. The authors declare no conflicts of interest.

Author contributions

C. G. H., C. J. H. and K. E. H. conceived and designed experiments. C. G. H., D. C. J., P. K. and P. K. did experiments. C. J. H. did mathematical modelling. All authors analysed data. C. G. H., C. J. H. and K. E. H. wrote the paper.

References

Adav, S.S., Ravindran, A., and Sze, S.K. (2012) Quantitative proteomic analysis of lignocellulolytic enzymes by *Phanerochaete chrysosporium* on different lignocellulosic biomass. *J Proteomics* **75:** 1493–1504.

Bietti, M., Baciocchi, E., and Steenken, S. (1998) Lifetime, reduction potential and base-induced fragmentation of the veratryl alcohol radical cation in aqueous solution. Pulse radiolysis studies on a ligninase 'mediator'. *J Phys Chem A* **102:** 7337–7342.

Blodig, W., Doyle, W.A., Smith, A.T., Winterhalter, K., Choinowski, T., and Piontek, K. (1998) Autocatalytic formation of a hydroxy group at Cβ of Trp171 in lignin peroxidase. *Biochemistry* **37:** 8832–8838.

Boerjan, W., Ralph, J., and Baucher, M. (2003) Lignin biosynthesis. *Annu Rev Plant Biol* **54:** 519–546.

Candeias, L.P., and Harvey, P.J. (1995) Lifetime and reactivity of the veratryl alcohol radical cation – implications for lignin peroxidase catalysis. *J Biol Chem* **270:** 16745–16748.

Cussler, E.L. (1984) *Diffusion: Mass Transfer in Fluid Systems*. Cambridge, UK: Cambridge University Press.

Daniel, G., Nilsson, T., and Pettersson, B. (1989) Intracellular and extracellular localization of lignin peroxidase during the degradation of solid wood and wood fragments by *Phanerochaete chrysosporium* by using transmission electron microscopy and immuno-gold labeling. *Appl Environ Microbiol* **55:** 871–881.

Daniel, G., Jellison, J., Goodell, B., Paszczynski, A., and Crawford, R. (1991) Use of monoclonal antibodies to

detect Mn(II)-peroxidase in birch wood degraded by *Phanerochaete chrysosporium*. *Appl Microbiol Biotechnol* **35:** 674–680.

Drummen, G.P.C., Gadella, B.M., Post, J.A., and Brouwers, J.F. (2004) Mass spectrometric characterization of the oxidation of the fluorescent lipid peroxidation reporter molecule C11-BODIPY581/591. *Free Radic Biol Med* **36:** 1635–1644.

Farrell, R.L., Blanchette, R.A., Brush, T.S., Hadar, Y., Iverson, S., Krisa, K., *et al*. (1993) Cartapip™ – a biopulping product for control of pitch and resin acid problems in pulp mills. *J Biotechnol* **30:** 115–122.

Fatin-Rouge, N., Milon, A., Buffle, J., Goulet, R.R., and Tessier, A. (2003) Diffusion and partitioning of solutes in agarose hydrogels: the relative influence of electrostatic and specific interactions. *J Phys Chem B* **107:** 12126–12137.

Fernandez-Fueyo, E., Ruiz-Duenas, F.J., Ferreira, P., Floudas, D., Hibbett, D.S., Canessa, P., *et al*. (2012) Comparative genomics of *Ceriporiopsis subvermispora* and *Phanerochaete chrysosporium* provide insight into selective ligninolysis. *Proc Natl Acad Sci USA* **109:** 5458–5463.

Halliwell, B., and Gutteridge, J.M.C. (1999) *Free Radicals in Biology and Medicine*. Oxford, UK: Oxford University Press.

Hammel, K.E., Kalyanaraman, B., and Kirk, T.K. (1986) Substrate free radicals are intermediates in ligninase catalysis. *Proc Natl Acad Sci USA* **83:** 3708–3712.

Harvey, P.J., Schoemaker, H.E., Bowen, R.M., and Palmer, J.M. (1985) Single-electron transfer processes and the reaction mechanism of enzymic degradation of lignin. *FEBS Lett* **183:** 13–16.

Harvey, P.J., Schoemaker, H.E., and Palmer, J.M. (1986) Veratryl alcohol as a mediator and the role of radical cations in lignin biodegradation by *Phanerochaete chrysosporium*. *FEBS Lett* **195:** 242–246.

Hatakka, A., and Hammel, K.E. (2010) Fungal biodegradation of lignocelluloses. In *The Mycota: Industrial Applications*. Hofrichter, M. (ed.). Berlin, Germany: Springer, pp. 319–340.

Henriksson, G., Zhang, L.M., Li, J.B., Ljungquist, P., Reitberger, T., Pettersson, G., and Johansson, G. (2000) Is cellobiose dehydrogenase from *Phanerochaete chrysosporium* a lignin degrading enzyme? *Biochim Biophys Acta* **1480:** 83–91.

Henriquez, C., Aliaga, C., and Lissi, E. (2002) Formation and decay of the ABTS derived radical cation: a comparison of different preparation procedures. *Int J Chem Kinet* **34:** 659–665.

Janse, B.J.H., Gaskell, J., Akhtar, M., and Cullen, D. (1998) Expression of *Phanerochaete chrysosporium* genes encoding lignin peroxidases, manganese peroxidases, and glyoxal oxidase in wood. *Appl Environ Microbiol* **64:** 3536–3538.

Kapich, A.N., Jensen, K.A., and Hammel, K.E. (1999) Peroxyl radicals are potential agents of lignin biodegradation. *FEBS Lett* **461:** 115–119.

Kersten, P., and Cullen, D. (2007) Extracellular oxidative systems of the lignin-degrading basidiomycete *Phanerochaete chrysosporium*. *Fungal Genet Biol* **44:** 77–87.

Kersten, P.J., Tien, M., Kalyanaraman, B., and Kirk, T.K. (1985) The ligninase of *Phanerochaete chrysosporium* generates cation radicals from methoxybenzenes. *J Biol Chem* **260:** 2609–2612.

Kirk, T.K., and Farrell, R.L. (1987) Enzymatic combustion – the microbial degradation of lignin. *Annu Rev Microbiol* **41:** 465–505.

Koduri, R.S., and Tien, M. (1994) Kinetic analysis of lignin peroxidise – explanation for the mediation phenomenon by veratryl alcohol. *Biochemistry* **33:** 4225–4230.

Krainev, A.G., and Bigelow, D.J. (1996) Comparison of 2,2′-azobis(2-amidinopropane) hydrochloride (AAPH) and 2,2′-azobis(2,4-dimethylvaleronitrile) (AMVN) as free radical initiators: a spin-trapping study. *J Chem Soc Perkin Trans* **2:** 747–754.

Kremer, S.M., and Wood, P.M. (1992) Production of Fenton reagent by cellobiose oxidase from cellulolytic cultures of *Phanerochaete chrysosporium*. *Eur J Biochem* **208:** 807–814.

Kuan, I.C., and Tien, M. (1993) Stimulation of Mn peroxidase activity – a possible role for oxalate in lignin biodegradation. *Proc Natl Acad Sci USA* **90:** 1242–1246.

Levesley, P., and Waters, W.A. (1955) Stages in oxidations of organic compounds by potassium permanganate. Part V. Oxidations of some α-hydroxy-acids by manganic pyrophosphate. *J Chem Soc***:** 217–221.

MacDonald, J., and Master, E.R. (2012) Time-dependent profiles of transcripts encoding lignocellulose-modifying enzymes of the white rot fungus *Phanerochaete carnosa* grown on multiple wood substrates. *Appl Environ Microbiol* **78:** 1596–1600.

MacDonald, J., Doering, M., Canam, T., Gong, Y.C., Guttman, D.S., Campbell, M.M., and Master, E.R. (2011) Transcriptomic responses of the softwood-degrading white-rot fungus *Phanerochaete carnosa* during growth on coniferous and deciduous wood. *Appl Environ Microbiol* **77:** 3211–3218.

Mahajan, S., and Master, E.R. (2010) Proteomic characterization of lignocellulose-degrading enzymes secreted by *Phanerochaete carnosa* grown on spruce and microcrystalline cellulose. *Appl Microbiol Biotechnol* **86:** 1903–1914.

Manavalan, A., Adav, S.S., and Sze, S.K. (2011) iTRAQ-based quantitative secretome analysis of *Phanerochaete chrysosporium*. *J Proteomics* **75:** 642–654.

Martinez, D., Larrondo, L.F., Putnam, N., Gelpke, M.D.S., Huang, K., Chapman, J., *et al*. (2004) Genome sequence of the lignocellulose degrading fungus *Phanerochaete chrysosporium* strain RP78. *Nat Biotechnol* **22:** 695–700.

Olsson, L.E., Westrin, B.A., Fransson, A., and Nordell, B. (1992) Diffusion of ferric ions in agarose dosimeter gels. *Phys Med Biol* **37:** 2243–2252.

Park, J.S.B., Wood, P.M., Davies, M.J., Gilbert, B.C., and Whitwood, A.C. (1997) A kinetic and ESR investigation of iron(II) oxalate oxidation by hydrogen peroxide and dioxygen as a source of hydroxyl radicals. *Free Radic Res* **27:** 447–458.

Popp, J.L., Kalyanaraman, B., and Kirk, T.K. (1990) Lignin peroxidase oxidation of Mn^{2+} in the presence of veratryl alcohol, malonic or oxalic acid, and oxygen. *Biochemistry* **29:** 10475–10480.

Ravalason, H., Jan, G., Molle, D., Pasco, M., Coutinho, P.M., Lapierre, C., *et al*. (2008) Secretome analysis of *Phanerochaete chrysosporium* strain CIRM-BRFM41 grown on softwood. *Appl Microbiol Biotechnol* **80:** 719–733.

Sato, S., Liu, F., Koc, H., and Tien, M. (2007) Expression analysis of extracellular proteins from *Phanerochaete chrysosporium* grown on different liquid and solid substrates. *Microbiology* **153:** 3023–3033.

Sato, S., Feltus, F.A., Iyer, P., and Tien, M. (2009) The first genome-level transcriptome of the wood-degrading fungus *Phanerochaete chrysosporium* grown on red oak. *Curr Genet* **55:** 273–286.

Srebotnik, E., and Messner, K. (1994) A simple method that uses differential staining and light microscopy to assess the selectivity of wood delignification by white-rot fungi. *Appl Environ Microbiol* **60:** 1383–1386.

Stewart, P., Whitwam, R.E., Kersten, P.J., Cullen, D., and Tien, M. (1996) Efficient expression of a *Phanerochaete chrysosporium* manganese peroxidase gene in *Aspergillus oryzae*. *Appl Environ Microbiol* **62:** 860–864.

Tanaka, H., Itakura, S., and Enoki, A. (1999) Hydroxyl radical generation by an extracellular low-molecular-weight substance and phenol oxidase activity during wood degradation by the white-rot basidiomycete *Phanerochaete chrysosporium*. *Holzforschung* **53:** 21–28.

Taube, H. (1948) The interaction of manganic ion and oxalate: rates, equilibria, and mechanism. *J Am Chem Soc* **70:** 1216–1220.

Tien, M., and Kirk, T.K. (1984) Lignin-degrading enzyme from *Phanerochaete chrysosporium* – purification, characterization, and catalytic properties of a unique H_2O_2-requiring oxygenase. *Proc Natl Acad Sci USA* **81:** 2280–2284.

Tien, M., and Kirk, T.K. (1988) Lignin peroxidase of *Phanerochaete chrysosporium*. *Methods Enzymol* **161:** 238–249.

Vallim, M.A., Janse, B.J.H., Gaskell, J., Pizzirani-Kleiner, A.A., and Cullen, D. (1998) *Phanerochaete chrysosporium* cellobiohydrolase and cellobiose dehydrogenase transcripts in wood. *Appl Environ Microbiol* **64:** 1924–1928.

Vanden Wymelenberg, A., Gaskell, J., Mozuch, M., Sabat, G., Ralph, J., Skyba, O., *et al*. (2010) Comparative transcriptome and secretome analysis of wood decay fungi *Postia placenta* and *Phanerochaete chrysosporium*. *Appl Environ Microbiol* **76:** 3599–3610.

Wariishi, H., Valli, K., and Gold, M.H. (1989) Oxidative cleavage of a phenolic diarylpropane lignin model dimer by manganese peroxidase from *Phanerochaete chrysosporium*. *Biochemistry* **28:** 6017–6023.

Wariishi, H., Valli, K., and Gold, M.H. (1992) Manganese(II) oxidation by manganese peroxidase from the basidiomycete *Phanerochaete chrysosporium* – kinetic mechanism and role of chelators. *J Biol Chem* **267:** 23688–23695.

Supporting information

Additional Supporting Information may be found in the online version of this article:

Fig. S1. a. Images showing changes in bead fluorescence after various extents of oxidation by *P. chrysosporium* on a wood section. From left to right, the RG ratios are 2.6, 1.5, and 1.0; and the corresponding concentrations of AAPH-derived radicals from the standard curve are 1, 10, and 25 mM. Each image frame is 5.8 μm wide.

b. Calibration curve relating RG ratios of BODIPY beads to concentrations of radicals generated by AAPH thermolysis. The points with error bars indicate experimental results with 95% confidence intervals, and the plotted curve is an empirical fit to the data using the equation shown.

Fig. S2. Relationship of predicted gradients in oxidant concentration to values of θ from the reaction–diffusion model.

Supplementary notes.

SUPPLEMENTARY INFORMATION

Spatial mapping of extracellular oxidant production by a white rot basidiomycete on wood reveals details of ligninolytic mechanism

Christopher G. Hunt, Carl J. Houtman, Don C. Jones, Peter Kitin, Premsagar Korripally, and Kenneth E. Hammel

US Forest Products Laboratory and Dept. of Bacteriology, University of Wisconsin, Madison, Wisconsin, USA

Supplementary Information Contains:

Supplementary Figures 1 and 2

Supplementary Notes

Supplementary References

SUPPLEMENTARY FIGURES

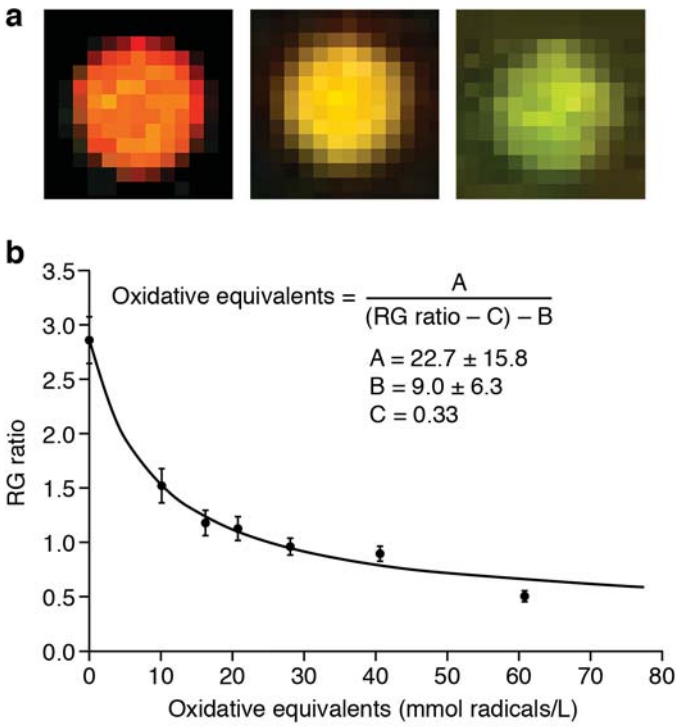

SUPPLEMENTARY FIGURE 1. a. Images showing changes in bead fluorescence after various extents of oxidation by *P. chrysosporium* on a wood section. From left to right, the RG ratios are 2.6, 1.5, and 1.0; and the corresponding concentrations of AAPH-derived radicals from the standard curve are 1, 10, and 25 mM. Each image frame is 5.8 µm wide. b. Calibration curve relating RG ratios of BODIPY beads to concentrations of radicals generated by AAPH thermolysis. The points with error bars indicate experimental results with 95% confidence intervals, and the plotted curve is an empirical fit to the data using the equation shown.

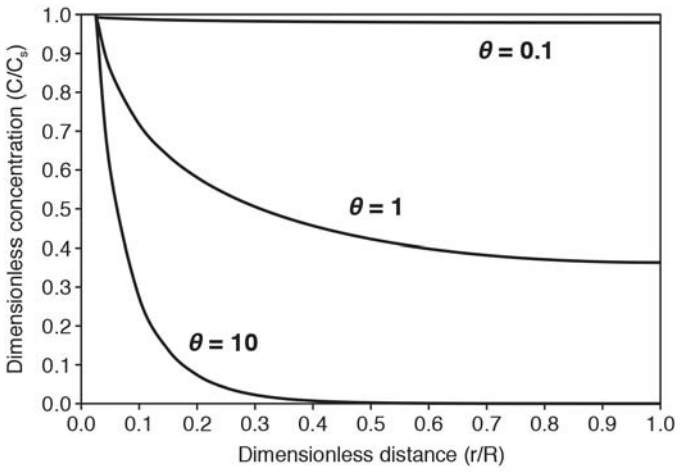

SUPPLEMENTARY FIGURE 2. Relationship of predicted gradients in oxidant concentration to values of θ from the reaction-diffusion model.

SUPPLEMENTARY NOTES

Bead properties. The RG ratios of the BODIPY beads were temperature-sensitive, and therefore the beads were stored at -80°C. The RG ratios also decreased if the beads became desiccated, and therefore care was taken during culture setup to mix the bead suspension with warm agarose solution immediately after the beads were placed on the glass cover slip. Finally, the RG ratios were sensitive to strong illumination, and therefore cultures containing beads were grown in dim light and examined by microscopy using a high numerical aperture objective. The RG ratios did not exhibit significant pH sensitivity over the physiological range of 3-7.

The quantity of BODIPY immobilized on the beads was approximately 2×10^{-4} molecules/nm^3. This load placed the dye molecules far enough apart (approx. 17 nm on average) to give a low probability of fluorescence resonance energy transfer (FRET), an undesired process for our purposes in which electronic energy on an oxidized dye molecule is transferred to an adjacent unreacted dye molecule that absorbs at a longer wavelength, thus reducing the shorter wavelength fluorescence that indicates the presence of oxidized dye (Lakowicz, 1983). Modeling of the response of our beads to oxidation indicated an approximately 10% probability that an oxidized BODIPY molecule fluorescing on an otherwise unoxidized bead would transfer its energy via FRET to an adjacent unoxidized BODIPY molecule. However, as oxidation proceeds, this probability is expected to decrease due to the depletion of unoxidized BODIPY molecules.

Bead calibration. The RG ratios obtained from measurements of bead fluorescence are not directly proportional to the number of dye molecule oxidations on each bead because the red reference fluorescence is not constant, but rather is depleted as the bead becomes more oxidized. Consequently, the decrease in RG ratio is more responsive to oxidative events at a low extent of bead oxidation than at a high extent.

An additional complication is oxidative biodegradation of the BODIPY dye by the fungus, which becomes significant once an experiment has proceeded long enough for a

significant proportion of the dye molecules to incur multiple random oxidative hits. As a result, some of the green fluorescence becomes depleted as bead oxidation progresses because multiple oxidations of a given BODIPY molecule destroy the dye, rendering it nonfluorescent.

Given these factors, the simplest way to relate RG ratios to the number of oxidations incurred is to apply an empirical standard curve obtained using a system that generates a known number of oxidants. This approach corrects for the more sensitive response of RG ratio changes at lower extents of oxidation and for the loss of green fluorescence that occurs at higher extents of oxidation. To correlate RG ratios with estimates of the quantity of oxidants produced in our culture system, we used the well-characterized thermolysis of 2,2'-azobis(2-methylpropionamidine) dihydrochloride (AAPH), which decays to give ultimately two peroxyl radicals (Krainev and Bigelow, 1996). The results do not provide absolute measurements of fungal oxidants—this is impossible in any case because the various candidates under consideration differ in reactivity—but by converting RG ratios to nominal peroxyl radical equivalents it is nonetheless possible to get rough estimates for the magnitude of oxidant production. Supplementary Figure 1a shows typical images of beads oxidized to various extents in a *P. chrysosporium* culture, and Supplementary Figure 1b shows a typical bead calibration curve. The average coefficient of variation for the RG ratio in a typical population of fresh, unoxidized beads was 23%.

Light microscopy. The procedure of Srebotnik and Messner (1994) was modified as follows: Wood sections recovered from cultures were (*a*) passed through an acetone series (30%, 50%, 75%, 100%, 75%, 50%, and 30%) to remove nonstructural phenolics and washed several times in water; (*b*) stained at room temperature for 3 to 5 min with 1% aqueous safranin-O; (*c*) rinsed with water until no leakage of dye was visible; (*d*) passed through an ethanol series (25%, 50%, 75%, 96%, 75%, 50%, and 30%) for at least one hour and several washes at each concentration until no leakage of dye was visible; (*e*)

washed several times in water; (*f*) stained with 1% aqueous astra-blue for 3 to 5 min; and (*g*) subjected again to the entire washing procedure outlined in steps *c*-*e*. The prepared wood sections were mounted in water and observed with an Olympus BX60 light microscope using bright-field optics.

Fluorescence microscopy. Since total fluorescence intensity decreases as the dye molecules incur multiple oxidative hits, laser power was increased to obtain data on more highly oxidized samples. The filter used to adjust laser intensity was found to have excellent linear response over the entire working range. In addition, since the red fluorescence of BODIPY decays more quickly than the green, independent control of the two excitation intensities was necessary to maximize the amount of data in each channel that was above the threshold level and below the saturation level. Typical values applied to unoxidized beads were 15 µs total scanning time per 0.45 µm pixel using 150 µW at 488 nm and 60 µW at 543 nm. For beads exposed to 40 mM AAPH-derived radicals or their equivalent in fungal oxidants, typical values increased to 375 µW and 350 µW, respectively.

Estimation of rate constants and diffusion constants. For hypothesis I, the Fenton reaction, we assumed that Fe(II) was present as the monooxalate complex and that H_2O_2 was present in large excess, because any other conditions would lead to lower reaction rates and thus to shallower gradients (Park et al., 1997). Similarly, for hypothesis II, the disproportionation of Mn(III) oxalate complexes, we assumed that only the monooxalate complex was present, because the more stable species containing multiple oxalates would lead to shallower gradients (Taube, 1948).

The free water diffusion coefficients (D_w) of [Fe(II) oxalate]^0 and [Mn(III) oxalate]$^{+1}$ were estimated using the Nernst-Haskel equation (Reid et al., 1977) and the limiting conductivities found in Coury (1999). These values were corrected from 25 to 38°C using the viscosity of water as suggested by Reid et al. (1977). To get the ratio of diffusion in agar (D_g) to the diffusion in free water (D_w), the measured value of the

diffusion coefficient for ferric sulfate (5.30×10^{-6} cm^2/s; Olsson et al., 1992) was divided by the estimate from the Nernst-Haskel equation (1.97×10^{-5} cm^2/s) for 25°C. The derived value of 0.27 indicated that the metal ions show some tendency to associate with the weakly charged agar.

For hypothesis III, the average D_w of LiPs (mol wt 38-46 kDa; Tien and Kirk, 1988) was estimated to be similar to that of ovalbumin (mol wt 45 kDa; Gibbs et al., 1991). This value was corrected from 25 to 38°C using the viscosity of water and the Wilke-Chang equation (Cussler, 1984). The D_g/D_w ratio was taken from Fatin-Rouge et al. (2003). The D_w of veratryl alcohol (hypothesis IV) was estimated using the modified Wilkie-Chang equation for aromatic compounds in water as described by Niesner and Heintz (2000). To account for the presence of the two methoxyl groups, a hard core volume of 29 cm^3/mol was added to the volume for *o*-cresol, 115 cm^3/mol, to obtain an estimate for veratryl alcohol. For purposes of our reaction-diffusion model, we are interested in the diffusion of the veratryl alcohol cation radical, but prior work suggests that diffusion coefficients for radicals are within 5% of values for their parent analogues (Donkers and Leaist, 1997). The D_g/D_w ratio was assumed to be 0.9, a typical value for small organic molecules (Fatin-Rouge et al., 2003).

The decay rate constants (K) for $[Fe(II)\ oxalate]^0$, $[Mn(III)\ oxalate]^{+1}$, and the veratryl alcohol cation radical (hypotheses I, II, and IV respectively) were taken from the literature (Taube, 1948; Candeias and Harvey, 1995; Park et al., 1997; Bietti et al., 1998). The temperature of these measurements is not given in the publications, so we assumed they were obtained at room temperature, correcting them from 25 to 38°C by assuming an activation energy of 50 kJ/mole. The decay rate of LiP (hypothesis III) was based on the observation that its activity does not change significantly on the time scale of a typical assay (Tien and Kirk, 1988). Assuming a conservative half-life of 1 h at 38°C, we get a K of 1.9×10^{-4} 1/s.

Propagation of uncertainty in calculated values of θ. As described above, a combination of experimental values and empirical correlation results was used to obtain values of for K, D_w and D_g/D_w, which were then used to calculate values of θ as shown in equation 1. Assuming that the variances in these parameters are uncorrelated, one can derive an equation for the estimated uncertainty in θ by calculating the partial derivative with respect to each parameter (Box et al., 1978). The equation, after rearrangement, is shown as equation 2.

$$\theta = \sqrt{\frac{K\,R^2}{\left(\frac{Dg}{Dw}\right)D_w}} \quad (1)$$

$$\frac{\Delta\theta}{\theta} = \sqrt{\frac{1}{4}\left(\frac{\Delta K}{K}\right)^2 + \frac{1}{4}\left(\frac{\Delta D_w}{D_w}\right)^2 + \frac{1}{4}\left(\frac{\Delta\left(\frac{D_g}{D_w}\right)}{\left(\frac{D_g}{D_w}\right)}\right)^2} \quad (2)$$

The uncertainties in the values of K for Mn(III)-oxalate, Fe(II)-oxalate and the veratryl alcohol cation radical, since not given in the literature, were assumed to be 10%. The uncertainty in K for the denaturation of LiP was assumed to be 100%. The uncertainty in diffusion coefficients determined by correlation has been determined to be 10% (Reid et al., 1977). The D_w value for LiP was estimated to be the same as that for a well-studied similarly sized protein, so its error is likely less than 5%. Finally, the uncertainty in D_g/D_w ratios is based on measured values and correlation values, and was assumed to have a typical uncertainty of 25%. The respective uncertainties in θ were estimated to be Fe(II) oxalate = 28%, Mn(III) oxalate = 17%, LiP = 52% and veratryl alcohol cation radical = 15%.

Mathematical derivation of reaction-diffusion model for fungal oxidants. If one assumes that the hypha produces an oxidant at its surface and this oxidant diffuses away uniformly in all directions, then the concentration profile will have an axis of symmetry collinear with the hypha. If an oxidant has a finite lifetime that can be characterized as

first-order decay, and if the hypha has a high aspect ratio, the concentration profiles will satisfy equation 3.

$$\frac{\partial C}{\partial t} = \frac{1}{r}\left(\frac{\partial}{\partial r}\left(rD\frac{\partial C}{\partial r}\right)\right) - KC \qquad (3)$$

In this equation, C is concentration that depends on time t and position r, D is the diffusion coefficient, and K is the first order rate constant for the oxidant decay. For this to be a well-posed problem we need to define initial and boundary conditions. By assuming that the surrounding medium has no oxidant initially, that the hypha produces a particular concentration of oxidant at its surface, and that there are other hyphae a particular distance away uniformly in all directions, we arrive at the following mathematical expressions for the initial and boundary conditions.

$$C(r, 0) = 0 \text{ for } r > R_o \qquad (4)$$

$$C(R_o, t) = C_s \text{ for } t > 0 \qquad (5)$$

$$\frac{\partial C(R,t)}{\partial r} = 0 \text{ for } t > 0 \qquad (6)$$

In these equations, C_s is the surface concentration, R_o is the radius of the hypha, and R is the half distance to the nearest hypha. Equation 6 expresses that at the boundary R there is no flux of oxidant across it, *i.e.,* beyond the boundary an identical hypha is producing the same level of oxidant.

It is instructive to transform these native equations into dimensionless form. The following new variables are defined, with the implicit assumption that D is uniform throughout the domain.

$$\varphi = \frac{C}{C_s};\ \rho = \frac{r}{R};\ \tau = \frac{tD}{R^2};\ \theta^2 = \frac{KR^2}{D}$$

Using these new variables, equation 3 becomes equation 7.

$$\frac{\partial \varphi}{\partial \tau} = \frac{1}{\rho}\left(\frac{\partial}{\partial \rho}\left(\rho\frac{\partial \varphi}{\partial \rho}\right)\right) - \theta^2\varphi \qquad (7)$$

For the particular problem of interest typical values of the parameters are R_o = 1 μm, R = 40 μm, $D = 1 \times 10^{-5}$ cm^2/sec, and t = 3 h. A calculation of dimensionless time, τ

= tR^2/D, gives a value of 6,570. Since this number is significantly greater than 1, one can assume the concentration profile has arrived to a steady state everywhere, and thus the time derivative is negligible. With this assumption, the partial differential equation 7 becomes the ordinary differential equation 8.

$$0 = \frac{d}{d\rho}\left(\rho \frac{d\varphi}{d\rho}\right) - \theta^2 \rho\varphi \text{ for } \rho \neq 0 \qquad (8)$$

Equation 8 is known as the modified Bessel's equation and has solutions in the form of I_o and K_o, which are the modified Bessel functions of zeroth order.

$$\varphi = A\, I_o(\theta\rho) + B\, K_o(\theta\rho) \qquad (9)$$

In equation 9, A and B are constants that can be determined by forcing the solution to meet the boundary conditions, $\varphi = 1$ for $\rho = \rho_o$ and $d\varphi/d\rho = 0$ for $\rho = 1$. Solving the resulting pair of equations, one can determine the values of A and B.

$$B = \frac{1}{K_o(\theta\rho_o) + \frac{I_o(\theta\rho_o)\,K_1(\theta)}{I_1(\theta)}} \qquad (10)$$

$$A = \frac{1 - BK_o(\theta\rho_o)}{I_o(\theta\rho_o)} \qquad (11)$$

Note that in equation 10, I_1 and K_1 are the modified Bessel functions of first order, which result from the differentiation of I_o and K_o with respect to ρ.

SUPPLEMENTARY REFERENCES

Bietti, M., Baciocchi, E., and Steenken, S. (1998) Lifetime, reduction potential and base-induced fragmentation of the veratryl alcohol radical cation in aqueous solution. Pulse radiolysis studies on a ligninase "mediator". *J. Phys. Chem. A* **102**: 7337-7342.

Box, G., Hunter, W., and Hunter, J. (1978) Statistics for Experimenters. New York: John Wiley and Sons.

Candeias, L.P., and Harvey, P.J. (1995) Lifetime and reactivity of the veratryl alcohol radical cation– implications for lignin peroxidase catalysis. *J. Biol. Chem.* **270**: 16745-16748.

Coury, L. (1999) Conductance measurements, part 1– theory. *Curr. Sep.* **18**: 91-96.

Donkers, R.L., and Leaist, D.G. (1997) Diffusion of free radicals in solution. TEMPO, diphenylpicrylhydrazyl, and nitrosodisulfonate. *J. Phys. Chem. B* **101**: 304-308.

Fatin-Rouge, N., Milon, A., Buffle, J., Goulet, R.R., and Tessier, A. (2003) Diffusion and partitioning of solutes in agarose hydrogels: The relative influence of electrostatic and specific interactions. *J. Phys. Chem. B* **107**: 12126-12137.

Gibbs, S.J., Chu, A.S., Lightfoot, E.N., and Root, T.W. (1991) Ovalbumin diffusion at low ionic strength. *J. Phys. Chem.* **95**: 467-471.

Krainev, A.G., and Bigelow, D.J. (1996) Comparison of 2,2'-azobis(2-amidinopropane) hydrochloride (AAPH) and 2,2'-azobis(2,4-dimethylvaleronitrile) (AMVN) as free radical initiators: A spin-trapping study. *J. Chem. Soc. Perkin Trans. 2*: 747-754.

Lakowicz, J.R. (1983) *Principles of Fluorescence Spectroscopy*. New York: Plenum Press.

Niesner, R., and Heintz, A. (2000) Diffusion coefficients of aromatics in aqueous solution. *J. Chem. Eng. Data* **45**: 1121-1124.

Olsson, L.E., Westrin, B.A., Fransson, A., and Nordell, B. (1992) Diffusion of ferric ions in agarose dosimeter gels. *Phys. Med. Biol.* **37**: 2243-2252.

Park, J.S.B., Wood, P.M., Davies, M.J., Gilbert, B.C., and Whitwood, A.C. (1997) A kinetic and ESR investigation of iron(II) oxalate oxidation by hydrogen peroxide and dioxygen as a source of hydroxyl radicals. *Free Rad. Res.* **27**: 447-458.

Reid, R.C., Prausnitz, J.M., and Sherwood, T.K. (1977) *Properties of Gases and Liquids*. New York: McGraw-Hill.

Srebotnik, E., and Messner, K. (1994) A simple method that uses differential staining and light microscopy to assess the selectivity of wood delignification by white-rot fungi. *Appl. Environ. Microbiol.* **60**: 1383-1386.

Taube, H. (1948) The interaction of manganic ion and oxalate: rates, equilibria, and mechanism. *J. Am. Chem. Soc.* **70**: 1216-1220.

Tien, M., and Kirk, T.K. (1988) Lignin peroxidase of *Phanerochaete chrysosporium*. *Methods Enzymol.* **161**: 238-249.